

Single-artificial-atom lasing using a voltage-biased superconducting charge qubit

S. Ashhab and Franco Nori

Frontier Research System, The Institute of Physical and Chemical Research (RIKEN),

Wako-shi, Saitama 351-0198, Japan and

Center for Theoretical Physics, Physics Department,

The University of Michigan, Ann Arbor, Michigan 48109-1040, USA

J. R. Johansson

Frontier Research System, The Institute of Physical and Chemical Research (RIKEN),

Wako-shi, Saitama 351-0198, Japan

A. M. Zagorskin

Frontier Research System, The Institute of Physical and Chemical Research (RIKEN),

Wako-shi, Saitama 351-0198, Japan and

Department of Physics, Loughborough University,

Loughborough LE11 3TU, United Kingdom

(Dated: December 1, 2018)

Abstract

We consider a system composed of a single artificial atom coupled to a cavity mode. The artificial atom is biased such that the most dominant relaxation process in the system takes the atom from its ground state to its excited state, thus ensuring population inversion. A recent experimental manifestation of this situation was achieved using a voltage-biased superconducting charge qubit. Even under the condition of ‘inverted relaxation’, lasing action can be suppressed if the ‘relaxation’ rate is larger than a certain threshold value. Using simple transition-rate arguments and a semiclassical calculation, we derive analytic expressions for the lasing suppression condition and the state of the cavity in both the lasing and suppressed-lasing regimes. The results of numerical calculations agree very well with the analytically derived results. We start by analyzing a simplified two-level-atom model, and we then analyze a three-level-atom model that should describe accurately the recently realized superconducting artificial-atom laser.

I. INTRODUCTION

Superconducting circuits have gained increased interest in recent years, particularly for their possible use in quantum information processing and as artificial atoms [1]. In relation to the artificial-atom concept, the idea of placing such an atom in contact with a harmonic-oscillator circuit element, which serves as a cavity, has attracted a great deal of attention [2]. Such circuit-QED systems hold promise for studying various quantum-optics phenomena in a highly controllable and easily tunable setting, as well as exploring parameter regimes that are inaccessible using natural atoms.

One of the most intriguing and counterintuitive phenomena in the fields of atomic physics and quantum optics is lasing [3]. Given the above-mentioned advantages of superconducting circuits for studying atomic-physics and quantum-optics phenomena, it is natural to investigate superconducting implementations of lasing. Indeed, there have been a number of recent theoretical proposals [4, 5, 6, 7, 8] and experimental demonstrations of lasing [9, 10] and population inversion [11] in superconducting systems.

In Ref. [4] a cyclically manipulated artificial atom is constantly driven into its excited state, from which it can relax by emitting a photon into the cavity, thus establishing a lasing state. In Ref. [6] an atom that is illuminated by an oscillating field with a properly chosen frequency emits photons into a low-frequency cavity. Here we analyze a situation that is different from both Refs. [4, 6], but is closer to the usual picture of lasing with natural atoms. Furthermore, the models that we study are closely related to the experiment of Ref. [9]. It should be mentioned here that similar models have been studied in the past in the study of single-atom lasing (see e.g. Refs. [12, 13]). A similar model was also analyzed in Ref. [5], but that paper explored different parameter regimes and analyzed different aspects of the problem from the present paper.

Using a transition-rate-based calculation, a semiclassical calculation and numerical simulations, we analyze the different possible states of the cavity as the system parameters are varied. Each one of the analytic calculations has its advantages. The transition-rate-based calculation derives in a transparent manner the lasing suppression condition and the state of the cavity deep in the lasing and the suppressed-lasing regimes. The semiclassical calculation provides a good approximation for the state of the cavity throughout the lasing state, but is not suited to analyze the suppressed-lasing regime, where it turns out that the state

of the cavity takes the form of a thermal state. For clarity, we start by analyzing a simplified two-level-atom model, and we later take the same approach to analyze a three-level-atom model that describes more accurately the experiment of Ref. [9]. In particular, we comment on a possible experimental implementation of the crossover between the lasing and thermal regimes with a superconducting artificial-atom laser.

II. TWO-LEVEL ATOM

In this section we analyze the simplified model where the atom contains two energy levels only. This model provides a good qualitative understanding of the mechanisms at play and the resulting phenomena in the experimental setup of interest to us. The qualitative understanding developed in this section will also be useful for identifying the importance of the different processes in the more realistic model analyzed in Sec. III below.

A. Model

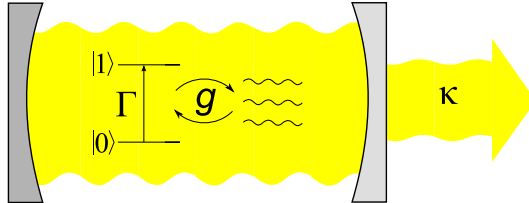


FIG. 1: (Color online) Schematic diagram of a two-level atom interacting with a cavity mode. The coupling strength for the exchange of excitations between the atom and the cavity is g . The atom is biased such that it experiences ‘inverted relaxation’ from the ground to the excited state, with rate Γ . The loss rate of photons out of the cavity is κ .

We consider the simple system composed of a two-level system interacting with a harmonic oscillator (which typically is one mode of an electromagnetic cavity). The system is shown schematically in Fig. 1. The Hamiltonian of the combined atom-cavity system is given by

$$\hat{H} = \frac{\hbar\omega_a}{2}\hat{\sigma}_z + \hbar\omega_0\hat{a}^\dagger\hat{a} + g\sigma_x(\hat{a} + \hat{a}^\dagger), \quad (1)$$

where ω_a is the atom’s characteristic frequency, ω_0 is the cavity’s natural frequency, g is the atom-cavity coupling strength, $\hat{\sigma}_x$ and $\hat{\sigma}_z$ are the usual Pauli matrices operating on the

atomic state, and \hat{a} and \hat{a}^\dagger are, respectively, the annihilation and creation operators acting on the state of the cavity. We shall describe quantum states using the notation $|n_a, n_c\rangle$, where $n_a = 0$ for the atomic ground state and $n_a = 1$ for the excited state, and n_c represents the number of photons in the cavity.

In order to have efficient emission of photons from the atom into the cavity, the atom and cavity frequencies must be almost equal. For the remainder of this paper, we shall take $\omega_a = \omega_0$. We also take this frequency to be the largest frequency (or energy) scale in the problem.

The setup is designed such that the atom's bias conditions cause it to 'relax' from the ground state to the excited state, with rate Γ [15]. In this section, the inverted relaxation is assumed as part of the theoretical model under consideration; a similar process will be derived from first principles in a realistic three-level-atom model in Sec. III. It is this counter-intuitive, inverted relaxation that will provide the mechanism for population inversion, which plays a crucial role in the realization of the lasing state. As such, one can say that the (usual) threshold condition for lasing action is automatically satisfied in this model. Note that we are ignoring any weak relaxation process pushing the atom from the excited to the ground state, since such a process would not affect the main points we wish to study. Furthermore, since the atom's relaxation rate will be taken to be very large, we shall ignore any additional atomic dephasing mechanisms. The cavity is taken to possess a decay rate κ .

An alternative description of the above situation concerning the bias conditions would be to say that the cavity is in contact with a heat bath that has a very small and positive temperature, while the atom is in contact with a heat bath that has a very small and negative temperature. It is worth mentioning here that a similar approach (with negative effective bath temperature) was used in Ref. [14] to describe an amplification process.

B. Photon emission and loss rates

In order to determine the state of the cavity for a given set of parameters, we first note that the above model contains a mechanism for photon emission into the cavity and a mechanism for photon loss from the cavity. We consider these two mechanisms separately.

The loss rate of photons from the cavity (i.e. the transition rate from the state $|n_a, n\rangle$ to the state $|n_a, n - 1\rangle$, where n_a represents the state of the atom) is given simply by the decay

rate κ multiplied by the number of photons in the cavity n :

$$\Gamma_{\text{loss}} = n\kappa. \quad (2)$$

Obtaining the photon emission rate requires a somewhat more careful analysis. We first consider the situation where there are no or few photons in the cavity. The atom's bias conditions constantly push it to its excited state. We can therefore assume the atom to be initially in the excited state. If the atom is in its excited state and the cavity has $n - 1$ photons, the atom-cavity coupling (with matrix element $g\sqrt{n}$) induces dynamics between the states $|1, n - 1\rangle$ and $|0, n\rangle$. Since $\Gamma \gg g$, the dynamics will take the form of an incoherent process described by the transition rate $W_{|1, n-1\rangle \rightarrow |0, n\rangle} = 4ng^2/\Gamma$. Any population that starts to accumulate in the state $|0, n\rangle$ will quickly relax to the state $|1, n\rangle$, because the atom is constantly pushed in this direction by its surrounding environment. These two steps complete the transition from the state $|1, n - 1\rangle$ to the state $|1, n\rangle$, or in other words, the process of adding one photon to the cavity. Since the upward-relaxation process occurs at a very large rate, it can be treated as being instantaneous. We therefore find that the photon emission rate (i.e. the transition rate from the state $|n_a, n - 1\rangle$ to the state $|n_a, n\rangle$) is given by the rate of the $|1, n - 1\rangle \rightarrow |0, n\rangle$ transition, i.e.

$$\Gamma_{\text{emission}} = \frac{4ng^2}{\Gamma}. \quad (3)$$

The photon emission rate therefore increases linearly with n for small values of n [19]. Clearly this situation cannot persist for large n , since this mechanism is ultimately limited by the atom's relaxation rate Γ . Indeed, when $g\sqrt{n}$ becomes comparable to or larger than Γ , the $|1, n - 1\rangle \leftrightarrow |0, n\rangle$ transitions must be treated as coherent oscillations. One can now argue that in the limit of very large n , where the system spends half of the time in each one of the two states ($|1, n - 1\rangle$ and $|0, n\rangle$), the atom has a chance to incoherently relax from its ground state into its excited state only half of the time. In this case the photon emission rate asymptotically reaches the value $\Gamma/2$, which it cannot exceed.

The main advantage of the above derivation of the photon emission rate is its simplicity, as well as the simplicity of the resulting expressions. A more detailed analysis of the photon emission rate for any value of n is possible, assuming that cavity is in a coherent (i.e. lasing) state. This calculation will be carried out in Sec. II.D below (see also [12, 16]).

C. Lasing condition and possible steady states

Combing the photon emission and loss rates as functions of photon number n , one can obtain the probability distribution of photon number states in the cavity. In particular, if this probability distribution has a peak for some value of n , the peak value can be obtained by locating the intersection point between the emission and loss rates. Some relevant examples of such a peak-finding calculation are depicted schematically in Fig. 2.

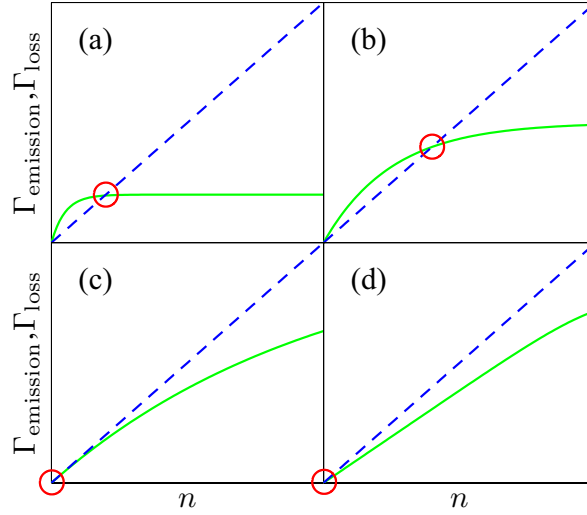


FIG. 2: (Color online) Schematic plot of the photon emission rate Γ_{emission} (green solid line) and the photon loss rate Γ_{loss} (blue dashed line) as functions of the photon number in the cavity n . The intersection point (red circle) determines the value of n in the photon-number probability distribution with the highest probability. Going from (a) to (d), Γ is increased, while κ is kept fixed.

We treat the atom's relaxation rate Γ as the tunable parameter, keeping g and κ fixed. From Eq. (3) one can see that small values of Γ correspond to a large initial slope of the emission rate (at $n = 0$), even though the emission rate reaches the saturation level for a relatively small value of n . Figure 2(a) represents this situation. If we increase Γ , the initial slope of the emission rate decreases, but it eventually reaches a larger value. By comparing Figs. 2(a) and 2(b), one can see that the peak value of the photon number in the cavity increases with increasing pumping rate. This result agrees with intuitive expectations.

A change of behaviour occurs when Γ reaches a certain regime, an expression for which

will be given shortly. As can be seen from Fig. 2(c), the peak value of n starts decreasing with increasing Γ and vanishes at a certain value of Γ . Beyond this point the value of n with maximum occupation probability remains at zero.

This suppression of lasing action by strong pumping is quite counterintuitive. It can be understood in terms of the quantum Zeno effect; at a certain point, the decoherence associated with pumping becomes the most dominant effect and inhibits the emission of photons from the atom into the cavity [17, 18]. In the following we shall analyze this effect, as well as the state of the cavity in the different regimes, more quantitatively.

By combining Eqs. (2) and (3), we find that if

$$\frac{4g^2}{\Gamma} > \kappa, \quad (4)$$

the photon emission rate is larger than the photon loss rate, assuming a small photon number in the cavity. Starting with a small photon number, the number increases exponentially in time [The growth in photon number continues until the peak value of n is reached, as represented by the circles in Figs. 2(a,b)]. If, on the other hand, Eq. (4) is not satisfied, the loss rate will be higher than the emission rate, and lasing would not occur. Equation (4) can therefore be considered a second threshold condition for lasing in this setup. Note that population inversion is guaranteed in this model and that all emission from the atom goes into the cavity.

We now consider the situation where the lasing condition (Eq. 4) is satisfied, and we analyze the probability distribution of the photon number in the cavity. Deep in the lasing regime, we can assume that the emission rate is well approximated by $\Gamma/2$. The loss rate is still given by Eq. (2). The peak in the photon-number probability distribution therefore occurs at

$$n_{\max} = \frac{\Gamma}{2\kappa}. \quad (5)$$

Note that this steady-state photon number is independent of the atom-cavity coupling strength. It is also worth mentioning that this relation remains valid even if Γ is smaller than g .

The width of the probability distribution can be calculated as follows. The ‘probability current’ from the $(n - 1)$ -photon state to the n -photon state is given by

$$W_{n-1 \rightarrow n} = \frac{\Gamma}{2} P_{n-1}, \quad (6)$$

whereas the probability current in the opposite direction is given by

$$\begin{aligned} W_{n \rightarrow n-1} &= n\kappa P_n \\ &= \frac{\Gamma}{2} P_n + (n - n_{\max}) \kappa P_n. \end{aligned} \quad (7)$$

Here P_n is the probability of having n photons in the cavity. Using the detailed balance equation, i.e. $W_{n-1 \rightarrow n} = W_{n \rightarrow n-1}$, the above two equations can be combined to give

$$\frac{P_n - P_{n-1}}{P_n} \approx -\frac{n - n_{\max}}{n_{\max}}, \quad (8)$$

which can be integrated to give the probability distribution

$$P_n = P_{\max} \exp \left\{ -\frac{(n - n_{\max})^2}{2n_{\max}} \right\}. \quad (9)$$

The width of the probability distribution is therefore of the order of $\sqrt{n_{\max}}$, as would be expected for the lasing state.

We now turn to the situation where lasing is suppressed, i.e. when $4g^2 < \Gamma\kappa$. In the linear regime (i.e. when n is small), we can write simple detailed balance equations for the probabilities P_n ;

$$\frac{P_{n+1}}{P_n} = \frac{\Gamma_{\text{emission}}(n)}{\Gamma_{\text{loss}}(n+1)} = \frac{4g^2}{\Gamma\kappa}. \quad (10)$$

This equation can be identified as the detailed-balance equation for a cavity in thermal equilibrium at effective temperature

$$T_{\text{eff}} = \frac{\hbar\omega_0}{k_B} \left[\log \left\{ \frac{\Gamma\kappa}{4g^2} \right\} \right]^{-1}. \quad (11)$$

Note that here we are neglecting the small ambient temperature of the cavity. Using the Bose-distribution formula, we find that the average number of photons at the above effective temperature is given by

$$\langle n \rangle = \left(\frac{\Gamma\kappa}{4g^2} - 1 \right)^{-1}. \quad (12)$$

Therefore, if we start from large values of Γ and we gradually decrease it, the average number of photons in the cavity starts increasing. This number follows a $1/x$ -type function that diverges at the threshold condition. The nonlinearity in the emission rate [see Fig. 2(c)] prevents the photon number from diverging at the critical value of Γ ; instead the system changes behaviour and enters the lasing regime.

D. Semiclassical derivation

In this subsection, we briefly review a mean-field approximation that can be used to find an analytic expression for the number of photons in the cavity in the lasing state. We follow closely the calculation of Ref. [12] (see also Ref. [18]): we write equations of motion for the expectation values of the relevant operators (in the rotating frame for simplicity), and from the stationary steady-state solution we extract the number of photons in the cavity.

We start with the Lindblad master equation for the model under consideration (see e.g. Ref. [14])

$$\begin{aligned} \frac{d\rho}{dt} = & -\frac{i}{\hbar} [\hat{H}, \rho] + \Gamma \left(\hat{\sigma}_+ \rho \hat{\sigma}_- - \frac{1}{2} \hat{\sigma}_- \hat{\sigma}_+ \rho - \frac{1}{2} \rho \hat{\sigma}_- \hat{\sigma}_+ \right) \\ & + \kappa \left(\hat{a} \rho \hat{a}^\dagger - \frac{1}{2} \hat{a}^\dagger \hat{a} \rho - \frac{1}{2} \rho \hat{a}^\dagger \hat{a} \right), \end{aligned} \quad (13)$$

where ρ is the total system's density matrix, and $\hat{\sigma}_\pm$ are the atom's raising and lowering operators. We can now multiply this equation on the left by any operator \hat{A} and take the trace over the density matrix. The result is an equation of motion for the average value of the operator \hat{A} , denoted $\langle A \rangle$.

The relevant equations of motion are:

$$\begin{aligned} \frac{d\langle a \rangle}{dt} &= g \langle \sigma_- \rangle - \frac{\kappa}{2} \langle a \rangle \\ \frac{d\langle \sigma_- \rangle}{dt} &= g \langle a \sigma_z \rangle - \frac{\Gamma}{2} \langle \sigma_- \rangle \\ \frac{d\langle \sigma_z \rangle}{dt} &= -2g \langle a^\dagger \sigma_- + a \sigma_+ \rangle + \Gamma (1 - \langle \sigma_z \rangle). \end{aligned} \quad (14)$$

Using the mean-field approximation (i.e. setting $\langle a \sigma_z \rangle = \langle a \rangle \langle \sigma_z \rangle$ etc.), choosing $\langle a \rangle$ to be real and setting the left-hand sides to zero (for the steady-state solution), we find for the average number of photons in the cavity (using the relation $\langle n \rangle = \langle a^2 \rangle$)

$$\langle n \rangle = \frac{\Gamma}{2\kappa} \left(1 - \frac{\Gamma\kappa}{4g^2} \right). \quad (15)$$

This expression is the mean-field approximation of the number of photons in the cavity. It predicts that deep in the lasing regime, i.e. when the second term inside the parentheses can be neglected, the number of photons will be given by $\Gamma/2\kappa$. It also predicts that the photon number will start decreasing with increasing Γ and will vanish when $\Gamma\kappa/(4g^2) = 1$. Both of these results agree with the results of Sec. II.C. Note that the semiclassical calculation

deals with average values, and therefore is not suited to describe the thermal state (which requires knowledge of the probability distribution of the photon occupation number in the cavity).

E. Numerical calculations

We now solve Eq. (13) numerically for different values of Γ , keeping g and κ fixed. As representative quantities that manifest the differences between the lasing and suppressed-lasing regimes, we plot in Fig. 3 the average photon number in the cavity $\langle n \rangle$ and the photon number with maximum probability n_{\max} as functions of the parameter $\Gamma\kappa/(4g^2)$.

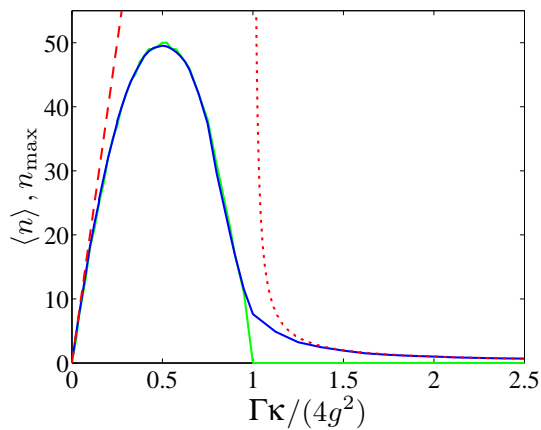


FIG. 3: (Color online) Average photon number $\langle n \rangle$ (blue solid line) and maximum-probability photon number n_{\max} (green solid line) in the cavity as functions of the parameter $\Gamma\kappa/(4g^2)$. Note that n_{\max} corresponds to red circles in Fig. 2. The values $g/\omega_0 = 8 \times 10^{-3}$ and $\kappa/\omega_0 = 5 \times 10^{-3}/(2\pi)$ were used in the numerical calculations. The red dashed line shows the predictions of Eq. (5) in the lasing regime, and the red dotted line shows the predictions of Eq. (12) in the thermal regime. The green line agrees very well with the predictions of the semiclassical calculation (Eq. 15).

The average photon number $\langle n \rangle$ agrees with the analytic expressions of Sec. II.C [Eqs. (5) and (12)] away from the threshold on both the lasing and thermal sides. The maximum-probability number n_{\max} agrees with the quadratic function derived in Sec. II.D (see also Ref. [12]) throughout the lasing regime. n_{\max} coincides with $\langle n \rangle$ deep in the lasing regime, but it decreases faster as the threshold is approached and clearly exhibits an abrupt change of behaviour when the threshold condition is crossed.

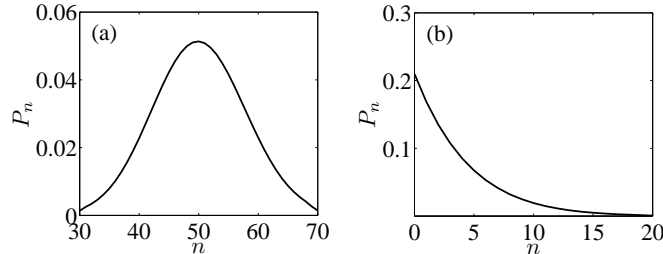


FIG. 4: Occupation probability as a function of photon number in the cavity for a point in the lasing regime (a; $\Gamma\kappa/(4g^2) = 0.5$) and one in the thermal regime (b; $\Gamma\kappa/(4g^2) = 1.25$). The system parameters are given in Fig. 3. The curve in (a) is fitted very well by a gaussian function, and the curve in (b) is fitted very well by a Boltzmann thermal-distribution function.

In Fig. 4 we plot the probability distribution of the photon number in the cavity for two points in Fig. 3, one in the lasing state and one in the thermal state. Apart from a small regime around the lasing-suppression threshold, the probability distribution is fitted very well by a gaussian function in the lasing regime and by an exponential (i.e. Boltzmann-distribution) function in the thermal regime.

III. THREE-LEVEL ATOM

We now consider a model that corresponds more closely to the experiment of Ref. [9], i.e. a Cooper-pair box coupled to a harmonic-oscillator circuit element. In the analogy with conventional lasers using natural atoms, the Cooper-pair box plays the role of the atom, whereas the linear circuit element plays the role of the cavity. We follow the methods explained in Sec. II above and apply them to this more realistic model with a three-level atom. It should be noted here that there has been some work in the past on single-atom lasers using three-level atoms or ions [12, 13]. The model we consider here, however, provides a more accurate description of the experimental situation of main interest to us [9].

A. Model

The Hamiltonian of the system is now given by

$$\hat{H} = \frac{\hbar\omega_a}{2} (\cos\theta\hat{\sigma}_z + \sin\theta\hat{\sigma}_x) + \hbar\omega_0\hat{a}^\dagger\hat{a} + g_0\sigma_z (\hat{a} + \hat{a}^\dagger), \quad (16)$$

where, as before, ω_a is the atom's characteristic frequency and ω_0 is the cavity's natural frequency, and these two frequencies are taken to be equal. The angle θ represents the deviation of the atom's bias point from the so-called degeneracy point, and g_0 is the atom-cavity coupling strength. In the three-level-atom model, the Pauli matrices $\hat{\sigma}_x$ and $\hat{\sigma}_z$ operate on the two active atomic states, with no need to include the third (inert) state explicitly in the Hamiltonian (in particular, the energy of the third state does not affect the results below).

A schematic diagram of the photon emission mechanism is shown in Fig. 5, including the dissipative processes. The state with $N + 1$ Cooper pairs in the box can relax to the state with N Cooper pairs and an unpaired electron in the box and an electron added to the drain electrode (this transition occurs with rate Γ_1). This state can relax further when the unpaired electron tunnels from the box into the drain electrode (with rate Γ_2). Once the box has N Cooper pairs and no unpaired electrons, its coupling to the source electrode allows a new Cooper pair to tunnel from the source electrode to the box.

One can now see how the inverted relaxation process occurs. Using an applied gate voltage to the Cooper-pair box, the system is biased such that the state with $N + 1$ Cooper pairs in the box is lower in energy than the state with N Cooper pairs, assuming a fixed number of electrons in the drain electrode. Under this condition, the state of the box with $N + 1$ Cooper pairs can, on a qualitative level, be identified as the ground state $|0\rangle$, and the state with N Cooper pairs in the box can be identified as the excited state $|1\rangle$. When the box starts in the state with $N + 1$ Cooper pairs and one electron tunnels out of the box into the drain electrode, the artificial atom goes from the ground state $|0\rangle$ to a third state that contains N Cooper pairs and one unpaired electron in the box. Barring coincidences, the extra unpaired electron in the box acts as an additional gate voltage, moving the Cooper-pair box away from the degeneracy point and from resonance with the cavity. As a result, this third level will not be involved in any coherent dynamics and can, for our purposes, be considered completely inert. Once in the inert state, the unpaired electron can tunnel from the box to the drain electrode and the atom relaxes to its excited state $|1\rangle$, thus completing the relaxation process. The fact that the states of the source and drain electrodes change during the relaxation processes, which is needed in order to ensure that energy is always lowered in each step of the relaxation process, does not need to be explicitly taken into account once we have established the mechanism for the inverted relaxation process in the

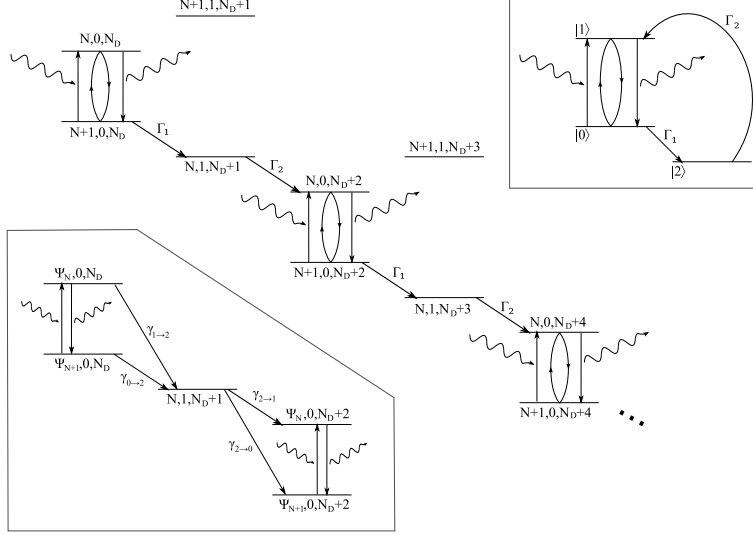


FIG. 5: The different processes involved in lasing for the experiment of Ref. [9]. The first, second and third quantum numbers represent, respectively, the number of Cooper pairs in the box, the number of unpaired electrons in the box and the number of electrons in the drain electrode. The box is resonantly coupled to a cavity mode, and the two can exchange excitations. The states with N and $N + 1$ Cooper pairs in the box are coupled because the box is biased in the vicinity of the so-called degeneracy point, so that Cooper pairs can tunnel coherently between the box and the source electrode. The system's total energy is lowered every time an electron tunnels (in a dissipative process) from the box to the drain electrode. The state with $N + 1$ Cooper pairs and a single unpaired electron in the box does not participate in the lasing mechanism. The inset in the bottom-left corner of the figure shows the same processes as in the main part of the figure, but in the energy eigenbasis of the Cooper-pair box. Because of the mixing between the Cooper-pair number states in the energy eigenstates of the box, the different relaxation rates shown in that inset obey the relations $\gamma_{0 \rightarrow 2} = \Gamma_1 \cos^2(\theta/2)$, $\gamma_{1 \rightarrow 2} = \Gamma_1 \sin^2(\theta/2)$, $\gamma_{2 \rightarrow 1} = \Gamma_2 \cos^2(\theta/2)$ and $\gamma_{2 \rightarrow 0} = \Gamma_2 \sin^2(\theta/2)$. The inset in the top-right corner of the figure shows a truncated model of a three-level atom where relaxation processes take the atom from the ground state ($|0\rangle$) to an inert state ($|2\rangle$) and then to the excited state ($|1\rangle$).

Cooper-pair box. Note that there are additional relaxation processes in Fig. 5, which occur because the ground and excited states of the box are superpositions of the states with N and $N + 1$ Cooper pairs in the box.

B. Photon emission and loss rates

The derivation of the emission rate is less straightforward in this case than the in Sec. II.B. Nevertheless, it can be done, and we carry it out here.

First we consider the small- n limit, where photon emission can be treated as an incoherent process. When the atom is in the state $|1\rangle$, the process by which it emits a photon into the cavity still occurs with the rate given by Eq. (3), noting that the relevant relaxation rate here is Γ_1 (which is the relaxation rate out of the space of active atomic states and represents the decoherence rate in that space) and now we have $g = g_0 \sin \theta$. One difference between the present case and that of Sec. II.B is that now the atom can undergo recurring transitions between the states $|0\rangle$, $|1\rangle$ and $|2\rangle$ even without the emission or absorption of photons. Therefore we need to include some additional arguments in order to take the above fact into account. When the atom is in the state $|0\rangle$, the process by which it absorbs a photon from the cavity occurs with the same rate as the one for photon emission. The net photon emission rate is therefore given by

$$\Gamma_{\text{emission}} = \frac{4ng^2}{\Gamma_1} (P_1 - P_0), \quad (17)$$

where P_j is the occupation probability of atomic state j . Using the relaxation rates shown in Fig. 5, we can derive the probabilities of the different states:

$$\begin{aligned} P_0 &= \frac{\tan^2 \frac{\theta}{2}}{\tan^2 \frac{\theta}{2} + \cot^2 \frac{\theta}{2} + \frac{\Gamma_1}{\Gamma_2}} \\ P_1 &= \frac{\cot^2 \frac{\theta}{2}}{\tan^2 \frac{\theta}{2} + \cot^2 \frac{\theta}{2} + \frac{\Gamma_1}{\Gamma_2}} \\ P_2 &= \frac{\Gamma_1/\Gamma_2}{\tan^2 \frac{\theta}{2} + \cot^2 \frac{\theta}{2} + \frac{\Gamma_1}{\Gamma_2}}, \end{aligned} \quad (18)$$

which gives

$$P_1 - P_0 = \frac{\cos \theta}{\cos^2 \theta + \left(\frac{1}{2} + \frac{\Gamma_1}{4\Gamma_2}\right) \sin^2 \theta}. \quad (19)$$

With this expression we find that the net emission rate in the small- n limit is given by

$$\Gamma_{\text{emission}} = \frac{4ng^2}{\Gamma_1} \left(\frac{\cos \theta}{\cos^2 \theta + \left(\frac{1}{2} + \frac{\Gamma_1}{4\Gamma_2}\right) \sin^2 \theta} \right). \quad (20)$$

Deep in the lasing regime, strong coupling with the cavity causes the atom to quickly reach equal populations of the states $|0\rangle$ and $|1\rangle$ every time it enters the space of active

states. Relaxation from the active space to the inert state therefore occurs with rate $\Gamma_1/2$. Relaxation from the inert state back to the active space occurs with rate Γ_2 . The atom's resetting rate (or Cooper-pair current) is therefore given by $(\Gamma_1/2) \times \Gamma_2 / (\Gamma_1/2 + \Gamma_2)$, which is the rate for a sequence of such recurrent relaxation steps. Since the atom has two possibilities when relaxing from the inert state to the active space [state $|1\rangle$ with probability $\cos^2(\theta/2)$ and state $|0\rangle$ with probability $\sin^2(\theta/2)$], the net photon emission rate will be given by

$$\Gamma_{\text{emission}} = \frac{(\Gamma_1/2) \times \Gamma_2}{\Gamma_1/2 + \Gamma_2} \times \cos \theta. \quad (21)$$

In the following subsection, we use the above rates to describe the state of the cavity.

C. Lasing condition and possible steady states

We can now follow the arguments of Sec. II.C with the expressions just derived in Sec. III.B and describe different properties of the system.

Setting the photon emission rate in the small- n limit (Eq. 20) equal to the photon loss rate (Eq. 2), we find the threshold condition

$$\frac{\Gamma_1 \kappa}{4g^2} = \frac{\cos \theta}{\cos^2 \theta + \left(\frac{1}{2} + \frac{\Gamma_1}{4\Gamma_2}\right) \sin^2 \theta}. \quad (22)$$

Deep in the lasing regime, equating the emission rate (Eq. 21) to the loss rate (Eq. 2) gives an average photon number of

$$\langle n \rangle = \frac{1}{\kappa} \frac{(\Gamma_1/2) \times \Gamma_2}{\Gamma_1/2 + \Gamma_2} \cos \theta. \quad (23)$$

In the suppressed-lasing regime, we find a thermal state with effective temperature

$$T_{\text{eff}} = \frac{\hbar\omega_0}{k_B} \left[\log \left\{ \frac{\Gamma_1 \kappa \cos^2 \theta + \left(\frac{1}{2} + \frac{\Gamma_1}{4\Gamma_2}\right) \sin^2 \theta}{4g^2 \cos \theta} \right\} \right]^{-1}. \quad (24)$$

Except for the above modified expressions, the qualitative physical description of the system remains essentially the same as the one given in Sec. II.C.

D. Semiclassical calculation

We now follow the semiclassical approach to derive the average photon number in the lasing state for the three-level-atom model. Using Eqs. (14) as a template and Fig. 5 as a guide for the relevant dissipative processes, we write the equations of motion:

$$\begin{aligned}
\frac{d\langle a \rangle}{dt} &= g \langle \sigma_- \rangle - \frac{\kappa}{2} \langle a \rangle \\
\frac{d\langle \sigma_- \rangle}{dt} &= g \langle a (P_1 - P_0) \rangle - \frac{\gamma_{0 \rightarrow 2} + \gamma_{1 \rightarrow 2}}{2} \langle \sigma_- \rangle \\
\frac{d(P_1 - P_0)}{dt} &= -2g \langle a^\dagger \sigma_- + a \sigma_+ \rangle + \gamma_{0 \rightarrow 2} P_0 - \gamma_{1 \rightarrow 2} P_1 + (\gamma_{2 \rightarrow 1} - \gamma_{2 \rightarrow 0}) (1 - P_0 - P_1) \\
\frac{d(P_1 + P_0)}{dt} &= -\gamma_{0 \rightarrow 2} P_0 - \gamma_{1 \rightarrow 2} P_1 + (\gamma_{2 \rightarrow 1} + \gamma_{2 \rightarrow 0}) (1 - P_0 - P_1), \tag{25}
\end{aligned}$$

where the γ s are the different relaxation rates, and σ_- transforms the state $|1\rangle$ into the state $|0\rangle$. Using the relations $\gamma_{0 \rightarrow 2} = \Gamma_1 \cos^2(\theta/2)$, $\gamma_{1 \rightarrow 2} = \Gamma_1 \sin^2(\theta/2)$, $\gamma_{2 \rightarrow 1} = \Gamma_2 \cos^2(\theta/2)$ and $\gamma_{2 \rightarrow 0} = \Gamma_2 \sin^2(\theta/2)$, the steady-state solution of the above equations gives

$$\begin{aligned}
\langle n \rangle &= \frac{1}{2\kappa} \left[\frac{\gamma_{0 \rightarrow 2} - \gamma_{1 \rightarrow 2} + 2\gamma_{2 \rightarrow 0} - 2\gamma_{2 \rightarrow 1}}{\gamma_{0 \rightarrow 2} + \gamma_{1 \rightarrow 2} + 2\gamma_{2 \rightarrow 0} + 2\gamma_{2 \rightarrow 1}} \left\{ \left(\frac{\gamma_{0 \rightarrow 2}^2}{4} - \frac{\gamma_{1 \rightarrow 2}^2}{4} \right) \frac{\kappa}{2g^2} + \gamma_{2 \rightarrow 0} + \gamma_{2 \rightarrow 1} \right\} \right. \\
&\quad \left. - \frac{(\gamma_{0 \rightarrow 2} + \gamma_{1 \rightarrow 2})^2}{4} \frac{\kappa}{2g^2} + \gamma_{2 \rightarrow 1} - \gamma_{2 \rightarrow 0} \right] \\
&= \frac{1}{2\kappa} \left[\frac{\Gamma_1 - 2\Gamma_2}{\Gamma_1 + 2\Gamma_2} \left\{ \frac{\Gamma_1^2 \kappa \cos \theta}{8g^2} + \Gamma_2 \right\} \cos \theta - \frac{\Gamma_1^2 \kappa}{8g^2} + \Gamma_2 \cos \theta \right] \\
&= \frac{\Gamma_1}{2\kappa} \left[\frac{1}{1 + \frac{\Gamma_1}{2\Gamma_2}} \cos \theta - \left(1 + \frac{1 - \frac{\Gamma_1}{2\Gamma_2}}{1 + \frac{\Gamma_1}{2\Gamma_2}} \cos^2 \theta \right) \frac{\Gamma_1^2 \kappa}{8g^2} \right]. \tag{26}
\end{aligned}$$

Equation (26) is clearly more complicated than Eq. (15), reflecting the more complicated nature of the two-step relaxation process in the three-level-atom model.

If we go deep into the lasing regime, i.e. by neglecting the terms containing $\Gamma_1 \kappa / g^2$ in Eq. (26), we recover Eq. (23). If we equate $\langle n \rangle$ to zero, we recover the threshold condition in Eq. (22). If we take the case where $\Gamma_1 = \Gamma_2$, Eq. (26) reduces to

$$\langle n \rangle = \frac{\Gamma_1}{2\kappa} \left[\frac{2}{3} \cos \theta - \frac{\Gamma_1 \kappa}{8g^2} \left(1 + \frac{1}{3} \cos^2 \theta \right) \right], \tag{27}$$

and the threshold condition is given by

$$\frac{\Gamma_1 \kappa}{4g^2} = \frac{4 \cos \theta}{3 + \cos^2 \theta}. \tag{28}$$

If we take the limit $\Gamma_2 \gg \Gamma_1$, Eq. (26) reduces to

$$\langle n \rangle = \frac{\Gamma_1}{2\kappa} \left[\cos \theta - \frac{\Gamma_1 \kappa}{8g^2} (1 + \cos^2 \theta) \right], \tag{29}$$

and the threshold condition is given by

$$\frac{\Gamma \kappa}{4g^2} = \frac{2 \cos \theta}{1 + \cos^2 \theta}. \tag{30}$$

For the parameters quoted in Ref. [9], i.e. $g = (2\pi) \times 44$ MHz, $\Gamma_1 = \Gamma_2 = (2\pi) \times 600$ MHz, $\kappa = (2\pi) \times 1.3$ MHz, $\theta = 0.18\pi$, one finds that the ratio $\Gamma_1\kappa/(4g^2) \approx 0.1$ (and $\langle n \rangle \approx 70$), with the threshold occurring at $\Gamma_1\kappa/(4g^2) \approx 0.9$. This set of parameters is therefore well inside the lasing regime. By reducing g and increasing κ (e.g. during fabrication), however, the boundary between the two regimes seems to be easily reachable. Since the pumping rate Γ is somewhat controllable in experiment, it should be possible to study the transition between the two regimes on a single sample.

E. Numerical calculations

We solve the quantum-optical master equation relevant to this model [which follows straightforwardly from Eq. (13) and Fig. 5] numerically for different values of Γ_1 , keeping g , κ and Γ_2/Γ_1 fixed. We plot in Fig. 6 the average photon number in the cavity $\langle n \rangle$ and the photon number with maximum probability n_{\max} as functions of $\Gamma_1\kappa/(4g^2)$. The main features in Fig. 6 are similar to those in Fig. 3, which is an indication that a good intuitive understanding of the system can be obtained from the simplified two-level-atom model. The curves in Fig. 6 also agree with the analytic expressions given in this section. We do not plot the probability distributions here because they look very similar to the ones shown in Fig. 4.

IV. CONCLUSION

We have analyzed the lasing behaviour of a single artificial atom in a cavity, in particular in connection with recent experiments on superconducting charge qubits. Although increased pumping strength initially results in a larger photon population in the cavity, increasing the pumping rate beyond a certain point starts to suppress the number of photons in the lasing state. When the pumping rate reaches a critical threshold value, lasing action is completely lost and a thermal state of the cavity is formed. We have analyzed the properties of both the lasing and suppressed-lasing (thermal) states. We have used a transition-rate-based approach, semiclassical calculations and numerical simulations in our analysis, and all three methods give consistent results. Our analysis and results are very relevant to the experimentally achieved situation of Ref. [9], suggesting that experimental tests of the

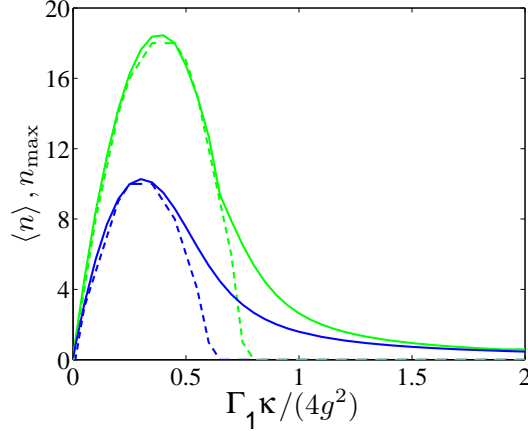


FIG. 6: (Color online) Average photon number $\langle n \rangle$ (solid lines) and maximum-probability photon number n_{\max} (dashed lines) in the cavity as functions of the parameter $\Gamma_1 \kappa / (4g^2)$. The values $g/\omega_0 = 8 \times 10^{-4}$, $\kappa/\omega_0 = 5 \times 10^{-4}/(2\pi)$ and $\theta = \pi/3$ were used in the numerical calculations. The ratio Γ_2/Γ_1 is 1 for the blue (black) lines and 10 for the green (gray) lines. All the numerical results agree well with theoretical predictions. The small difference between the solid and dashed lines deep in the lasing regime is due to the discreteness of n_{\max} .

phenomena studied in this paper should be possible in the near future.

Acknowledgments

We would like to thank A. Abdumalikov, O. Astafiev, P. Berman, A. Fedorov, Y. Nakamura, A. Satanin and A. Smirnov for useful discussions. This work was supported in part by the National Security Agency (NSA), the Laboratory for Physical Sciences (LPS), the Army Research Office (ARO), the National Science Foundation (NSF) grant No. EIA-0130383, the JSPS-RFBR 06-02-91200 and Core-to-Core (CTC) program supported by the Japan Society for Promotion of Science (JSPS).

-
- [1] For recent reviews on the subject, see e.g. J. Q. You and F. Nori, *Phys. Today* **58** (11), 42 (2005); G. Wendin and V. Shumeiko, in *Handbook of Theoretical and Computational Nanotechnology*, ed. M. Rieth and W. Schommers (ASP, Los Angeles, 2006); J. Clarke and F. K. Wilhelm, *Nature* **453**, 1031 (2008).

- [2] I. Chiorescu, P. Bertet, K. Semba, Y. Nakamura, C. J. P. M. Harmans, and J. E. Mooij, *Nature* **431**, 159 (2004); A. Wallraff, D. I. Schuster, A. Blais, L. Frunzio, R. S. Huang, J. Majer, S. Kumar, S. M. Girvin, and R. J. Schoelkopf, *Nature* **431**, 162 (2004); J. Johansson, S. Saito, T. Meno, H. Nakano, M. Ueda, K. Semba, and H. Takayanagi, *Phys. Rev. Lett.* **96**, 127006 (2006).
- [3] See e.g. P. W. Milonni and J. H. Eberly, *Lasers* (Wiley, New York, 1988); M. O. Scully and M. S. Zubairy, *Quantum Optics* (Cambridge University Press, 1997); L. Davidovich, *Rev. Mod. Phys.* **68**, 127 (1996); W. E. Lamb, W. P. Schleich, M. O. Scully, and C. H. Townes, *Rev. Mod. Phys.* **71**, S242 (1999).
- [4] J. Q. You, Y.-X. Liu, C. P. Sun, and F. Nori, *Phys. Rev. B* **75**, 104516 (2007).
- [5] D. A. Rodrigues, J. Imbers, and A. D. Armour, *Phys. Rev. Lett.* **98**, 067204 (2007).
- [6] J. Hauss, A. Fedorov, C. Hutter, A. Shnirman, and G. Schön, *Phys. Rev. Lett.* **100**, 037003 (2008).
- [7] O. V. Zhirov and D. L. Shepelyansky, *Phys. Rev. Lett.* **100**, 014101 (2008).
- [8] An early proposal for a Josephson-junction-based maser was given in N. Hatakenaka and S. Kurihara, *Phys. Rev. A* **54**, 1729 (1996); *Czech. J. Phys.* **46**, 2311 (1996).
- [9] O. Astafiev, K. Inomata, A. O. Niskanen, T. Yamamoto, Yu. A. Pashkin, Y. Nakamura, and J. S. Tsai, *Nature* **449**, 588 (2007).
- [10] M. Grajcar, S. H. W. van der Ploeg, A. Izmailkov, E. Il'ichev, H.-G. Meyer, A. Fedorov, A. Shnirman, G. Schön, *Nature Physics* **4**, 612 (2008).
- [11] D. M. Berns, M. S. Rudner, S. O. Valenzuela, K. K. Berggren, W. D. Oliver, L. S. Levitov, and T. P. Orlando, *Nature* **455**, 51 (2008).
- [12] Y. Mu and C. M. Savage, *Phys. Rev. A* **46**, 5944 (1992).
- [13] H.-J. Briegel and B.-G. Englert, *Phys. Rev. A* **47**, 3311 (1993); C. Ginzler, H.-J. Briegel, U. Martini, B.-G. Englert, and A. Schenzle, *Phys. Rev. A* **48**, 732 (1993); T. Pellizzari and H. Ritsch, *J. Mod. Opt.* **41**, 609 (1994); G. M. Meyer, H.-J. Briegel, and H. Walther, *Europhys. Lett.* **37**, 317 (1997); G. M. Meyer, M. Löffler, and H. Walther, *Phys. Rev. A* **56**, 1099 (1997); G. M. Meyer and H.-J. Briegel, *PRA* **58**, 3210 (1998).
- [14] C. W. Gardiner and P. Zoller, *Quantum Noise* (Springer, Berlin, 2000).
- [15] Note that we do not use any factors of 2π with decay rates. In other words, the occupation probability of the atom's ground state decreases in time as $\exp\{-\Gamma t\}$.

- [16] T. H. Stoof and Yu. V. Nazarov, Phys. Rev. B **53**, 1050 (1996).
- [17] A number of other situation where the quantum Zeno effect plays an interesting role in superconducting circuits have been analyzed recently; See e.g. X.-B. Wang, J. Q. You, and F. Nori, Phys. Rev. A **77**, 062339 (2008); F. Helmer, M. Mariani, E. Solano, and F. Marquard, arXiv:0712.1908.
- [18] A similar effect was also predicted in the study of electronic transport through double quantum dots; S. A. Gurvitz, Phys. Rev. B **57**, 6602 (1998); see also S. A. Gurvitz and Ya. S. Prager, Phys. Rev. B **53**, 15932 (1996); G. Cohen, S. A. Gurvitz, I. Bar-Joseph, B. Deveaud, P. Bergman, and A. Regreny, Phys. Rev. B **47**, 16012 (1993).
- [19] Note that the reason for the appearance of the relaxation rate on the right-hand side of Eq. (3) is that it represents the decoherence rate between the two atomic states. Any relevant pure dephasing rate would also be added to the decoherence rate entering this calculation.